Intelligent and Sustainable Manufacturing

SCIEPublish

Article

Gradient Fabrication of Cu-Zn Alloy Coating and Synergistic Anti-Corrosion Mechanism of Carbon Layer

Keke Jiang [1], Yongqiang Fu [2], Ying Fu [1,3], Yanbin Zhang [2], Xing Zhao [4], Xuesong Chang [4], Tiewei Liu [4], Dongzhou Jia [1,5,*] and Xiaoqiang Wu [6,*]

[1] College of Mechanical Engineering and Automation, Liaoning University of Technology, Jinzhou 121001, China; jiangkeke2023@163.com (K.J.); zkcm-fuying@zkcrystal.com (Y.F.)
[2] School of Mechanical and Automotive Engineering, Qingdao University of Technology, Qingdao 266520, China; yqfu@nuaa.edu.cn (Y.F.); zhangyanbin1_QDLG@163.com (Y.Z.)
[3] Songshan Lake Materials Laboratory, Dongguan 523808, China
[4] Hisense Home Appliances Group Co., Ltd., Qingdao 266000, China; zhaoxing2@hisense.com (X.Z.); changxuesong@hisense.com (X.C.); liutiewei@hisense.com (T.L.)
[5] College of Interdisciplinary Sciences, Liaoning University of Technology, Jinzhou 121001, China
[6] College of Mechanical and Traffic Engineering, Ordos Institute of Technology, Ordos 017000, China

* Corresponding author. E-mail: jia_dongzhou@163.com (D.J.); wangzai8402@163.com (X.W.)

Received: 18 April 2026; Revised: 7 July 2026; Accepted: 18 September 2026; Available online: 24 September 2026

ABSTRACT: Due to their dense microstructure and excellent thickness controllability, copper films are widely utilized in flexible electronics and energy storage device systems. Their interfacial stability in electrochemical environments becomes the critical factor limiting device cycle life and safety. However, in fluorine-containing electrolyte environments, copper is susceptible to severe HF-induced corrosion, generating unstable products such as CuF_2, which can lead to structural degradation and functional failure. The results indicated that the film with a low Zn content (Cu-Zn (9.5:0.5 wt%)) exhibited deteriorated corrosion resistance due to a significant micro-galvanic effect. Its corrosion current was as high as 6.87×10^{-5} mA·cm^{-2}. By contrast, the high-Zn-content film (Cu-Zn (9:1 wt%)) formed a composite passivation film that increased charge transfer resistance to 1.22×10^4 Ω·cm^2 and reduced the corrosion current to 2.08×10^{-5} mA·cm^{-2}. The introduction of an additional carbon layer resulted in optimal stability of the Cu-Zn (9:1 wt%)@C composite film, with the corrosion current decreasing to 6.14×10^{-6} mA·cm^{-2} and the structure remaining intact after corrosion. Multi-scale characterization revealed that the addition of zinc to the alloy enhanced the film's intrinsic passivation capability, while the carbon layer provided an external barrier effect through physical isolation, charge regulation, and stress relief. This synergy effectively suppressed the formation of by-products. In summary, the Cu-Zn (9:1 wt%)@C composite film demonstrated the greatest corrosion resistance, establishing a theoretical foundation and engineering approach for the design of highly stable metallic films for use in intricate electrochemical environments.

Keywords: Cu-Zn alloy composite passivation layer; Alloy proportion control; Interfacial stability; Electrochemical corrosion mechanism

1. Introduction

With the rapid advancement in flexible electronics, miniaturized sensors, and energy storage devices, the stability of metallic films in complex electrochemical environments has garnered increasing attention [1–3]. Prolonged exposure of these films to electrolytes in such environments often triggers corrosion and interfacial degradation, leading to structural deterioration and performance decline [4,5]. Due to their low cost, advanced processing techniques, and excellent mechanical properties, copper and its alloys are widely used in polymer-based flexible films and microdevice structures [6,7]. Nevertheless, they exhibit pronounced susceptibility to corrosion in fluoride-containing electrolytes, which facilitates the formation of unstable by-products such as CuO or CuF_2, thereby destroying interfacial stability [8,9]. This problem not only affects the long-term reliability of copper alloy films in flexible device and sensor packaging but also limits their potential applications in energy storage system architecture protection [10]. Consequently, enhancing the corrosion resistance of copper alloy films in electrolyte environments has become a pivotal research focus in the field of materials corrosion and protection, and it holds profound significance for the development of advanced composite films that integrate both flexibility and high stability.

In order to solve the corrosion problem of copper film in fluorine-containing electrolyte environment, researchers have proposed two main strategies: regulating the coating's alloy and constructing a protective surface layer [11–13]. The alloy ratio control is to form a solid solution or intermetallic compound by adding elements such as zinc (Zn), tin (Sn), and aluminum (Al) to copper, thereby adjusting the intrinsic electrochemical potential and improving the interfacial reaction kinetics [11–16]. For instance, brass (a Cu-Zn alloy) is widely utilized due to its comprehensive performance. The introduction of Zn can preferentially react with aggressive anions via the "sacrificial anode effect", thereby inhibiting the direct dissolution of copper (Cu) [17–19]. On one hand, the selective dissolution of Zn promotes the formation of a Cu-rich sub-layer at the alloy-electrolyte interface, which acts as an electrochemically inert barrier to shield the substrate. In the Cu-Zn system, Zn has a more negative electrode potential than Cu, and can be preferentially dissolved as a sacrificial anode in the electrolyte containing F, thereby protecting the Cu matrix [20]. Concurrently, a composite Cu-Zn oxide film provides the basis for passivation [21,22]. On the other hand, the influence of Zn content on corrosion resistance is non-monotonic. An overabundance of Zn (>30–40 wt%) accelerates dezincification and can foster the growth of more electrochemically active microstructures, such as the β-phase, severely compromising the alloy's defense against localized corrosion [21,23]. Conversely, a Zn-deficient composition fails to generate a sufficiently dense and continuous protective architecture, neither the Cu-rich sub-layer nor the oxide film, leading to impaired protection, with performance potentially falling below that of pure copper under specific conditions [24]. Therefore, meticulous compositional engineering is paramount to developing high-performance, corrosion-resistant copper alloys [20,22]. The second strategy, surface modification, involves fabricating a physically or chemically stable protective layer on the copper surface, such as graphene, amorphous carbon, polymers, or self-assembled monolayers, to act as a physical barrier against the ingress of corrosive media [25–27]. For example, Kim et al. enhanced both interfacial adhesion and stability by modifying a copper surface with graphene via chemical vapor deposition [25]. Han et al. introduced three-dimensional carbon nanowalls onto a copper current collector, which significantly delayed electrolyte attack while causing almost no reduction in electrical conductivity [27]. Alloying enhances corrosion resistance by modulating the material's internal electrochemical properties, whereas surface coatings provide protection by establishing an external barrier against corrosive media [28–30]. Although each strategy has its merits, their individual application face limitations, particularly under complex service conditions such as those involving flexible polymer substrates [31–35]. In these scenarios, materials are often subjected to a combination of bending, stretching, and electrochemical corrosion, rendering their interfacial stability even more fragile [36–40]. Consequently,

developing a multi-faceted protection strategy that integrates both internal and external approaches has become a critical issue that urgently needs to be addressed.

Based on the aforementioned multi-dimensional data analysis and comprehensive assessment, this study proposes a hybrid approach that synergistically combines two strategies: alloying and surface coating modification. Initially, magnetron sputtering is employed to fabricate Cu and Cu-Zn films on a flexible polyimide (PI) substrate, with the aim of systematically elucidating the effect of Zn content on corrosion performance. Subsequently, a protective carbon layer is introduced onto the surface of the Cu-Zn film that exhibits optimal corrosion resistance, thereby constructing a composite structure that possesses both high corrosion resistance and potential for flexibility. This composite design is not only anticipated to achieve a synergistic protective effect—yielding a "1 + 1 > 2" outcome—but also offers a novel research avenue for enhancing the long-term reliability of copper alloy films in the fields of flexible electronics and energy storage protection.

2. Materials and Methods

2.1. Preparation of Composite Copper Foil

In this study, the films were fabricated on 25 μm thick flexible polyimide (PI) substrates using magnetron sputtering. As shown in Figure 1, utilizing a pulsed power supply (200 W, −60 V bias), films with an approximate thickness of 1 μm were deposited over an hour period from pure Cu, Cu-Zn (9:1 wt%), and Cu-Zn (9.5:0.5 wt%) films. Following a comparative evaluation of their corrosion performance, the Cu-Zn (9:1 wt%) film was identified as exhibiting the optimal resistance and was subsequently selected for further modification. A carbon layer approximately 100 nm in thickness was then deposited onto its surface by sputtering for an hour using a DC power supply (200 W, −10 V bias), ultimately forming the Cu-Zn (9:1 wt%)@C composite film.

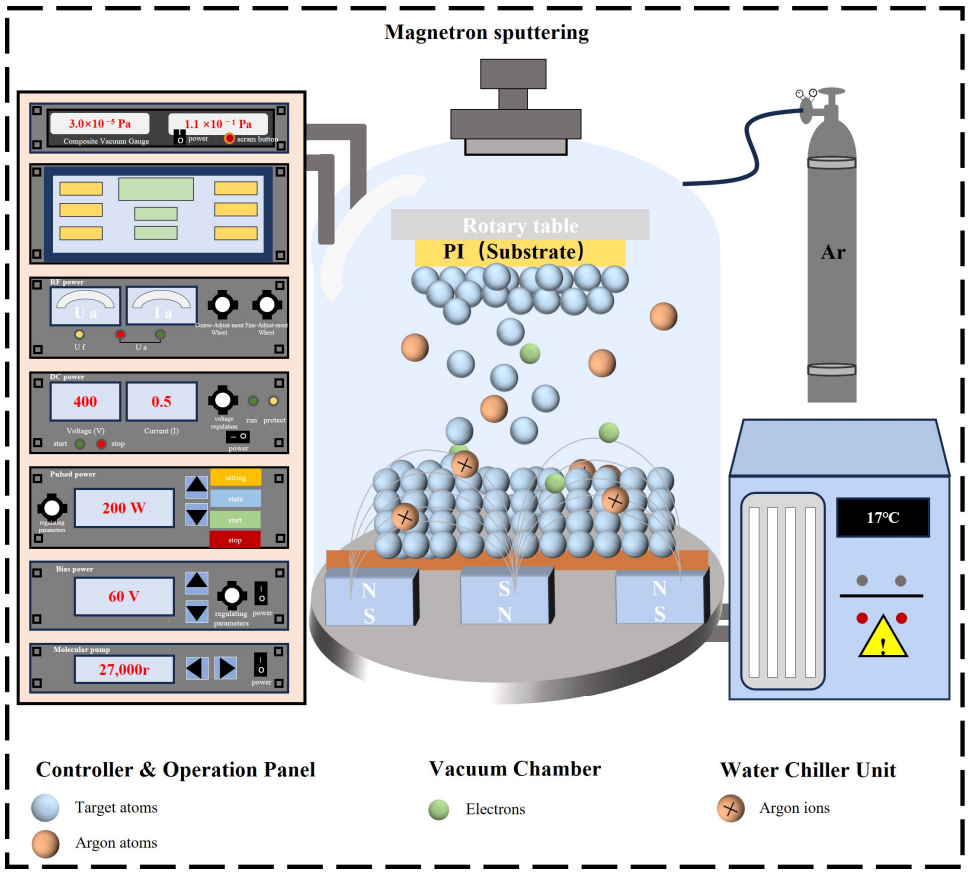

Figure 1. Schematic diagram of the film's preparation process by magnetron sputtering.

2.2. Electrochemical Measurements

To systematically probe the electrochemical corrosion behavior of the composite films, all measurements were conducted in a sealed polypropylene cell featuring a three-electrode configuration. As shown in Figure 2, an external potential was applied to mimic the corrosive conditions inherent to battery charge-discharge cycling. The prepared composite film was used as the working electrode (WE) with an exposed geometric area of 1 cm × 1 cm (1 cm^2), while a silver chloride (Ag/AgCl) electrode and a platinum (Pt) plate were used as the reference electrode (RE) and counter electrode (CE), respectively. The electrolyte consisted of 1 mol/L $LiPF_6$ dissolved in a mixed solvent of ethylene carbonate (EC), ethyl methyl carbonate (EMC), and dimethyl carbonate (DMC) with a volume ratio of 1:1:1. The commercial battery-grade $LiPF_6$ electrolyte (purity ≥ 99.9%) was prepared and transferred in an Ar-filled glove box with moisture and oxygen levels below 0.1 ppm. The solvents were pretreated with molecular sieves to reduce moisture contamination, and the water content was controlled below 20 ppm. The three-electrode system assembly and electrolyte injection were performed in the glove box, while all film samples were vacuum-dried at 60 °C for 12 h before transfer to remove adsorbed moisture. Electrochemical Impedance Spectroscopy (EIS) and potentiodynamic polarization (Tafel) tests were carried out using an electrochemical workstation (CS350M, Wuhan Corrtest Instruments Corp., Ltd., Wuhan, China).

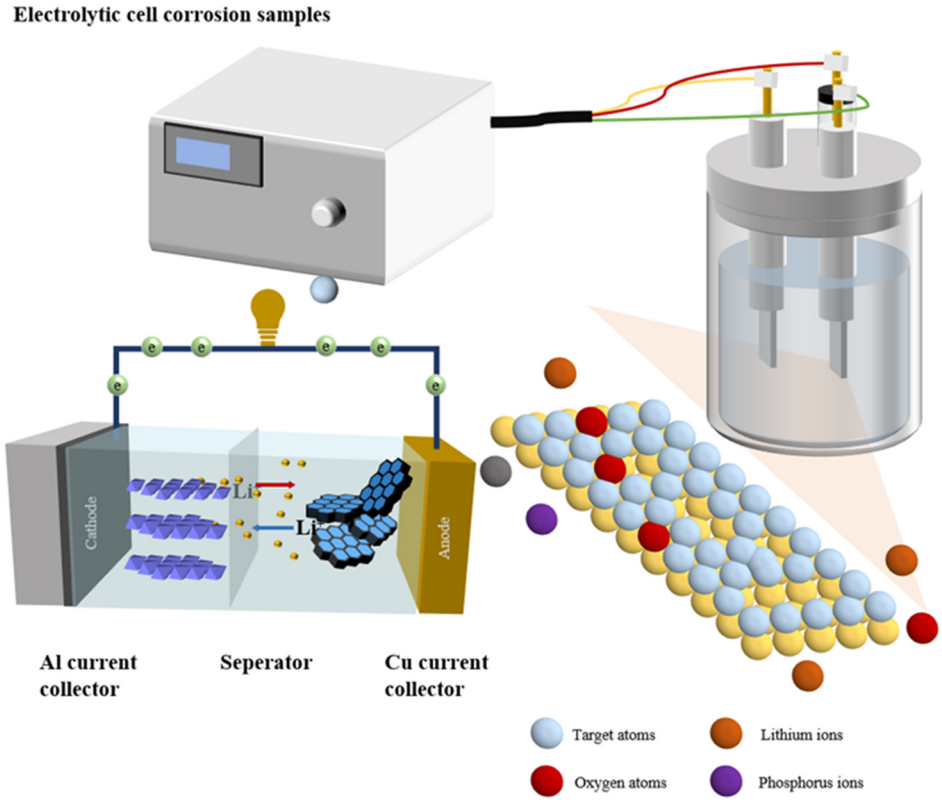

Figure 2. Schematic diagram of the electrochemical corrosion testing apparatus and the corrosion mechanism of the current collector.

2.3. Materials Characterization

To systematically evaluate the multi-scale properties of the films, a series of characterization methods was employed in this study. A Field Emission Scanning Electron Microscope (FE-SEM) equipped with an Energy Dispersive Spectrometer (EDS) was used to characterize the surface morphology and elemental distribution. The film substrate interfacial bonding strength was quantitatively measured using a multi-function material surface property tester (MFT-4000 Lanzhou Huahui Instrument Technology Co., Ltd.,

Lanzhou, China), and the initial surface roughness was measured with an Atomic Force Microscope (AFM-Cypher S). Subsequently, the corrosion resistance of each sample was evaluated through electrochemical experiments. After the corrosion tests, the samples were ultrasonically cleaned with anhydrous ethanol and dried for post-corrosion analysis. SEM and EDS were used again to observe the evolution of the corroded morphology and the redistribution of elements, while AFM was used to quantify the change in surface roughness after corrosion. To further reveal the corrosion mechanism, X-ray Photoelectron Spectroscopy (XPS) was utilized for an in-depth analysis of the chemical composition and elemental valence states of the corrosion products. Concurrently, X-ray Diffraction (XRD) was employed to identify the phase structure of these products.

3. Results and Discussion

3.1. Characterization of Initial Surface Morphology

$LiPF_6$ is the most common electrolyte used in commercial lithium-ion batteries. Its primary function is to facilitate the migration of lithium ions (Li^+) between the cathode and anode, which directly impacts the battery's energy density, cycle life, and safety. Although other lithium salts exist, such as bistrifluoromethanesulfonimide lithium salt (LiTFSI) and lithium bis (fluorosulfonyl) imide (LiFSI), $LiPF_6$ remains the market's preferred choice due to its performance advantages. Nevertheless, $LiPF_6$ exhibits poor chemical stability and is highly susceptible to hydrolysis during electrolyte storage or cycling, leading to the formation of hydrogen fluoride (HF). The generated HF not only instigates detrimental side reactions with the electrode materials but also induces severe corrosion of the copper foil current collector, consequently diminishing interfacial stability and curtailing the battery's operational lifespan.

To elucidate the differential resistance to HF corrosion among various material systems, this study initiated a comparative analysis of the pre-corrosion surface morphology and elemental composition of several composite films. As shown in Figure 3a,c,e,g, the pre-corrosion surface morphologies and corresponding elemental mappings of the different composite films. As observed, the surfaces of all four samples are comparatively flat and smooth, devoid of any discernible corrosion features. As shown in Figure 3b,d,f,h, the compositional structures of the samples are clearly delineated. Sample 1 is a pure copper (Cu) film, Sample 2 is a copper-zinc (Cu-Zn (9:1 wt%)) alloy, Sample 3 is a copper-zinc (Cu-Zn (9.5:0.5 wt%)) film, and Sample 4 is a copper-zinc (Cu-Zn (9:1 wt%)@C) composite film, which was fabricated by applying a carbon coating to the surface of the Cu-Zn (9:1 wt%) film.

3.2. Film-Substrate Adhesion

The adhesion between the film and the substrate is a critical factor in determining the long-term service reliability of flexible devices. Figure 4 shows the results of the scratch tests for the four films. By observing the scratch morphology and determining the critical load (Lc_2) at which large-scale delamination of the film begins, the film-substrate adhesion strength can be evaluated (ISO 20502). The Lc_2 of the pure Cu film is 4.38 N, the Cu-Zn (9:1 wt %) film is 4.25 N, the Cu-Zn (9.5:0.5 wt%) film is 4.22 N, and the Cu-Zn (9:1 wt%)@C composite film is 4.38 N. This indicates that they all form a robust bond with the PI substrate and that the introduction of the functional carbon layer did not come at the expense of mechanical adhesion.

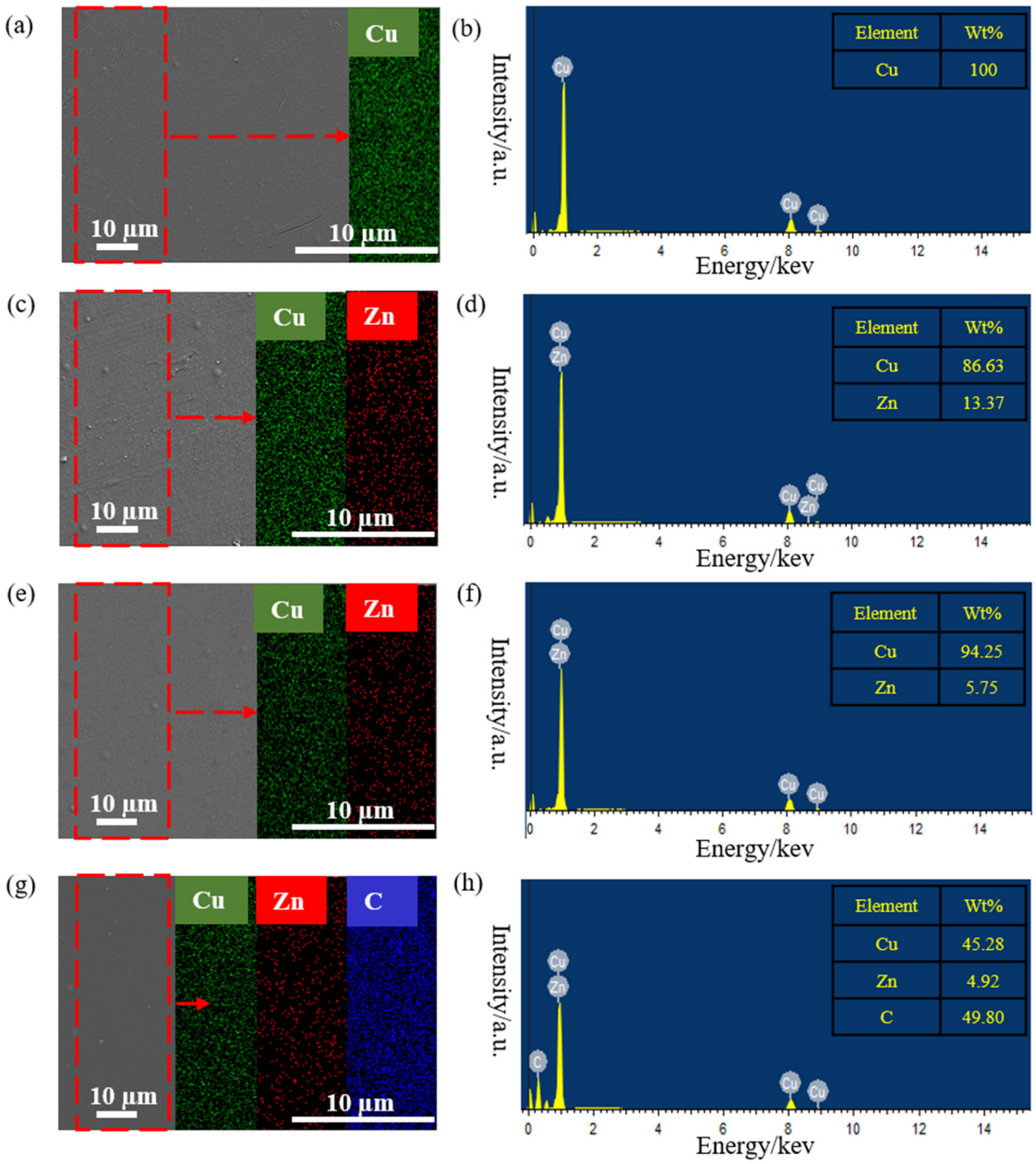

Figure 3. The surface morphology and elemental composition analysis results of the four films before corrosion. (**a**) and (**b**) are the SEM morphology (including Cu element distribution map) and EDS energy spectrum of pure copper film, respectively; (**c**) and (**d**) are the SEM morphology of Cu-Zn (9:1 wt%) film (including the distribution map of Cu and Zn elements) and its EDS energy spectrum; (**e**) and (**f**) are the SEM morphology of Cu-Zn (9.5:0.5 wt%) film (including the distribution map of Cu and Zn elements) and its EDS energy spectrum;(**g**) and (**h**) are the SEM morphology of Cu-Zn (9:1 wt%)@C composite film (including Cu, Zn, C element distribution map) and its EDS energy spectrum.

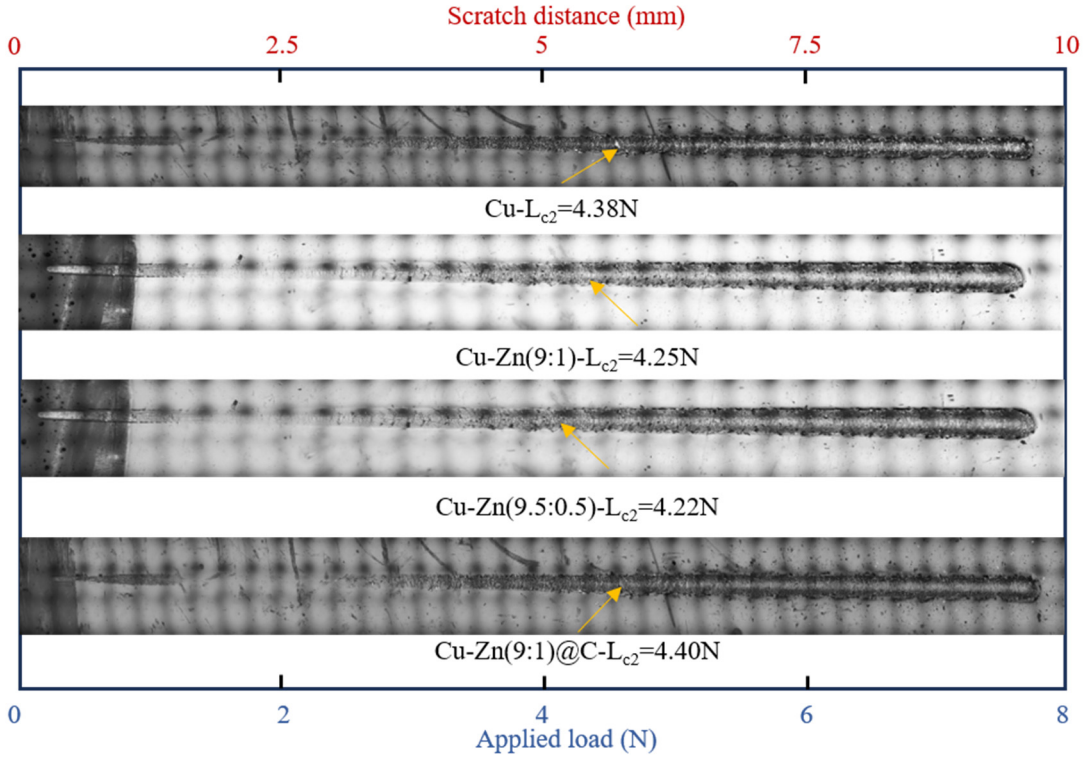

Figure 4. Scratch test morphologies and critical loads of Cu film, Cu-Zn (9:1 wt%) film, Cu-Zn (9.5:0.5 wt%) film, and Cu-Zn (9:1 wt%)@C composite film before corrosion.

3.3. Electrochemical Testing

To further quantify the differences in corrosion resistance among the four films, a systematic evaluation was conducted using EIS and Tafel techniques. The EIS test is carried out at an open circuit potential with a frequency range of 10^{-2} Hz to 10^{5} Hz and an AC amplitude of 10 mV. The scanning rate of the Tafel polarization curve is 2 mV·s^{-1}. All tests were performed at room temperature (25 ± 1 °C). The corrosion immersion test lasted for 24 h without applying potential. In the equivalent circuit, R_s is the solution resistance, R_f and Q_f represent the resistance and capacitance of the surface film (passivation film or carbon layer), R_{ct} and Q_{dl} represent the charge transfer resistance and double layer capacitance. The results of the EIS tests are presented in Figure 5 and Table 1. The differences in corrosion resistance among the various composite films are primarily manifested in the variations of the interfacial charge transfer resistance (R_{ct}). The R_{ct} of pure Cu film was only 6.76 × 10^3 Ω·cm^2, indicating limited interfacial impedance. This allows fluoride ions to easily penetrate the surface passivation layer and participate in electrochemical reactions, accelerating the dissolution of the substrate. In contrast, the R_{ct} of Cu-Zn (9.5:0.5 wt%) film decreased to 1.24 × 10^3 Ω·cm^2. This shows that the non-uniform distribution of a small amount of Zn produces a potential difference on the surface, which induces local micro-galvanic corrosion, making the charge more easily transmitted at the grain boundary and the defect area, and thus the corrosion resistance is worse. When the Zn content was increased to form the Cu-Zn (9:1 wt%) film, the R_{ct} significantly increased to 1.22 × 10^4 Ω·cm^2. This increase of nearly an order of magnitude is attributed to the higher proportion of Zn, which enables the formation of a dense ZnO or CuO composite passivation film on the surface. This film effectively blocks the direct attack of F^- on the substrate and greatly increases the difficulty of charge transfer, thereby significantly improving corrosion resistance. After further constructing a carbon layer on its surface, the R_{ct} of the Cu-Zn (9:1 wt%)@C composite film increased further to 1.47 × 10^4 Ω·cm^2. On one hand, the carbon layer acts as a dense physical barrier, reducing electrolyte penetration. On the other hand, its flexible buffering properties weaken the damage to the passivation film caused by volume

expansion and stress concentration during the corrosion process, while also regulating the interfacial charge distribution to suppress the formation of active sites. Through repeated verification and cross-comparison of extensive experimental data, it was demonstrated that Cu-Zn (9:1 wt%)@C composite film exhibits optimal impedance performance. This reflects a multi-synergistic protective mechanism of "interfacial isolation, charge blocking, and stress relief".

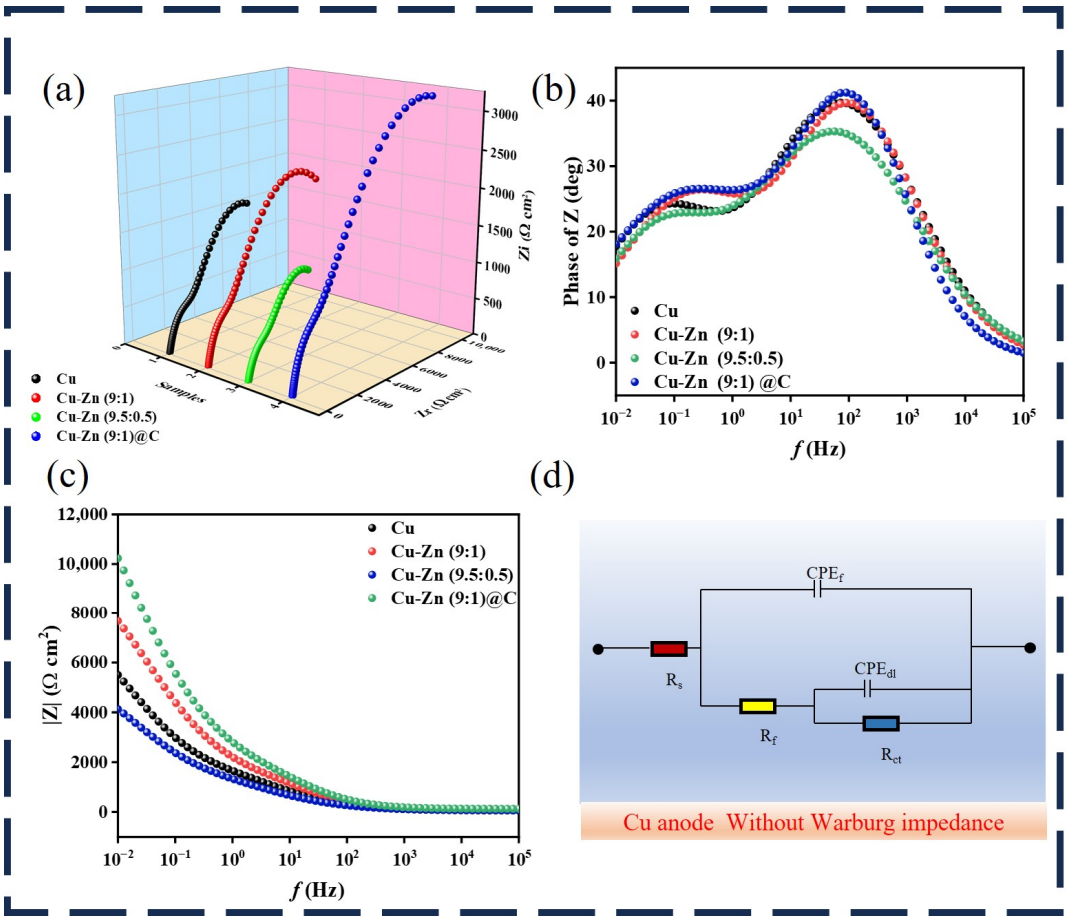

Figure 5. EIS results of Cu film, Cu-Zn (9:1 wt%) film, Cu-Zn (9.5:0.5 wt%) film, and Cu-Zn (9:1 wt%)@C composite film after corrosion: (**a**) Nyquist plots, (**b**,**c**) Bode plots, and (**d**) the equivalent circuit model used for fitting.

Table 1. EIS fitting data of four types of film samples.

Sample	R_s (Ω·cm²)	Q1-Y (F/cm²)	Q1-n (F/cm²)	R (Ω·cm²)	Q2-Y (F/cm²)	Q2-n (F/cm²)	R_{ct} (Ω·cm²)
S1	6.18×10^{1}	8.13×10^{-5}	6.09×10^{-1}	1.24×10^{3}	6.19×10^{-4}	5.85×10^{-1}	6.75×10^{3}
S2	9.30×10^{1}	2.83×10^{-5}	6.77×10^{-1}	1.42×10^{3}	2.66×10^{-4}	4.42×10^{-1}	1.22×10^{4}
S3	6.35×10^{1}	8.17×10^{-4}	5.80×10^{-1}	1.03×10^{3}	7.34×10^{-4}	5.55×10^{-1}	1.24×10^{3}
S4	1.28×10^{2}	2.30×10^{-5}	7.01×10^{-1}	1.88×10^{3}	2.31×10^{-4}	4.98×10^{-1}	1.47×10^{4}

Note: The units for Q-Y and Q-n are F·cm^{-2}, while the unit for R is Ω·cm^{2}. The sample designations are as follows: S1 (pure Cu film), S2 (Cu-Zn (9:1 wt%) film), S3 (Cu-Zn (9.5:0.5 wt%) film), and S4 (Cu-Zn (9:1 wt%)@C composite film).

As shown in Figure 6, the Tafel results further reveal the differences in thermodynamic stability and kinetic behavior of corrosion among the various samples. Table 2 presents the fitted parameters from the potentiodynamic polarization curves. Among these, the E_{corr} is the potential at which the sample's surface achieves electrochemical equilibrium. At this potential, the anodic dissolution and cathodic reduction reactions of the corrosion process are balanced, which allows for the determination of the i_{corr}. The corrosion current density is regarded as one of the most important indicators for judging a material's corrosion resistance. The smaller the corrosion current density, the slower the corrosion rate, and the better the corrosion resistance.

The E_{corr} for pure Cu film, Cu-Zn (9.5:0.5 wt%) film, Cu-Zn (9:1 wt%) film, and Cu-Zn (9:1 wt%)@C composite film were 0.257, 0.207, 0.349, and 0.448 V, respectively. The progressive positive shift in the E_{corr} values indicates that the tendency for corrosion is gradually suppressed. Furthermore, the i_{corr} for pure Cu film, Cu-Zn (9.5:0.5 wt%) film, Cu-Zn (9:1 wt%) film, and Cu-Zn (9:1 wt%)@C composite film were 4.09×10^{-5}, 6.87×10^{-5}, 2.08×10^{-5}, and 6.14×10^{-6} mA·cm^{-2}, respectively. These values also demonstrate that Cu-Zn (9:1 wt%)@C composite film possesses excellent corrosion resistance.

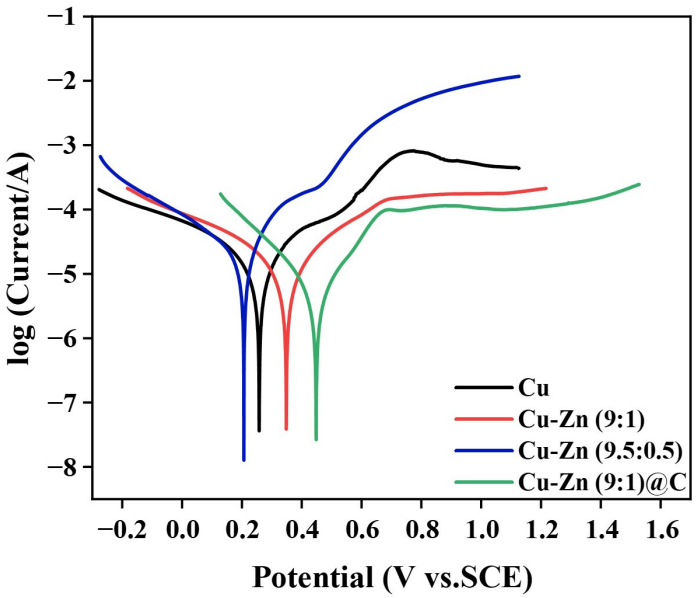

Figure 6. Tafel curves of Cu film, Cu-Zn (9:1 wt%) film, Cu-Zn (9.5:0.5 wt%) film, and Cu-Zn (9:1 wt%)@C composite film after corrosion.

Table 2. The Tafel parameters for the four films samples of table.

Sample	E_{ocp} (V)	i_{corr} (mA·cm^{-2})	E_{corr} (V)
S1	0.322	4.08×10^{-5}	0.257
S2	0.416	2.08×10^{-5}	0.348
S3	0.326	6.87×10^{-5}	0.206
S4	0.728	6.14×10^{-6}	0.448

Note: The sample designations are as follows: S1 (Cu film), S2 (Cu-Zn (9:1 wt%) film), S3 (Cu-Zn (9.5:0.5 wt%) film), and S4 (Cu-Zn (9:1 wt%)@C composite film).

In order to systematically evaluate the trade-off between corrosion resistance and electrical properties, the resistivity of four thin film samples was tested by four-probe method (RTS-9) at room temperature. The results show that the pure Cu film has the lowest resistivity of 3.09×10^{-5} Ω·cm. The resistivity of the Cu-Zn (9.5:0.5 wt%) film is 1.5×10^{-4} Ω·cm, and the resistivity of Cu-Zn (9:1 wt%) films increased to 1.97×10^{-3} Ω·cm, which was mainly attributed to the enhancement of electron scattering caused by the solid solution strengthening of Zn solute atoms in Cu matrix. It is worth noting that the resistivity of the Cu-Zn (9:1 wt%)@C composite film obtained by coating a carbon layer of about 100 nm on the surface of the Cu-Zn (9:1 wt%) film is 2.06×10^{-3} Ω·cm, which is basically the same as that of the alloy substrate without carbon coating (1.97×10^{-3} Ω·cm), only increased by about 4.6%. The dense carbon layer does not have a significant adverse effect on the overall conductivity of the film while exerting the physical barrier function. Although the resistivity of Cu-Zn (9:1)@C composite film is still higher than that of pure Cu, it can be seen from the electrochemical test results that the corrosion current density is one order of magnitude lower than that of pure Cu, and the charge transfer resistance is significantly increased,which relative to the uncoated

alloy substrate is consistent with previous reports on carbon/copper composite systems [41,42], where carbonaceous protective layers were shown to enhance corrosion resistance without severely compromising electrical conductivity. These studies demonstrated that an integrated assessment—balancing barrier efficiency against conductor-level performance—is essential for current-collector applications [41,42]. The present results confirm that the 100 nm carbon layer satisfies this requirement, achieving a substantial gain in corrosion resistance at the expense of only limited conductivity degradation. It can be seen that the corrosion resistance and interface stability of the composite film have been greatly improved under the premise of only sacrificing limited conductivity. For the current collector of flexible electronic devices and energy storage devices, long-term chemical stability and corrosion resistance are often the key factors that determine the service life and safety of devices. Therefore, the Cu-Zn (9:1)@C composite film achieves a good balance between conductivity and corrosion resistance, and has practical application value.

3.4. Analysis of Corrosion Products

To systematically evaluate the corrosion resistance conferred by different alloying strategies, the pure Cu, Cu-Zn (9:1 wt%), and Cu-Zn (9.5:0.5 wt%) films were treated under identical corrosion conditions. Following treatment, the samples were removed and ultrasonically cleaned with ethanol before being immediately subjected to SEM characterization, as shown in Figure 7. The unmodified pure Cu film (as shown in Figure 7a) and the low-zinc-content Cu-Zn (9.5:0.5 wt%) film (Figure 7e) both exhibited significant localized corrosion. The surface of the pure Cu developed a high density of diffusely distributed etch pits, whereas the corrosion on the Cu-Zn (9.5:0.5 wt%) film was more severe, presenting as large-area etch pits in localized regions. In contrast, the Cu-Zn (9:1 wt%) film (Figure 7c) demonstrated markedly superior corrosion resistance compared to the other two. Its surface revealed only minor traces of corrosion, with the overall morphology remaining largely intact. This validates the beneficial effect of an optimized alloying ratio in enhancing the stability of the copper alloy films. It is noteworthy that the Cu-Zn (9:1 wt%)@C composite film current collector (Figure 7g) exhibited virtually no discernible changes under the same conditions, its surface state was highly consistent pre- and post-corrosion. This indicates that the introduction of the carbon layer effectively impedes the corrosion reaction, thereby further augmenting the material's chemical stability.

A comparison of the EDS analysis results before and after corrosion (Figures 3 and 7) clearly elucidates the significant differences in the elemental composition and evolutionary patterns among the various samples. Prior to corrosion, the pure Cu film consisted solely of the Cu element, exhibiting a monolithic surface composition. Upon the introduction of Zn, both Cu and Zn were detected in the Cu-Zn (9:1 wt%) and Cu-Zn (9.5:0.5 wt%) films, with the Zn content varying in accordance with the alloy ratio. For the Cu-Zn (9:1 wt%) film with a carbon overlayer, a high proportion of the C element was detected, indicating that the carbon layer had been uniformly deposited onto the alloy surface. Subsequent to the corrosion treatment, the presence of C, O, F, and trace amounts of P was observed on all samples, which indicates that HF participated in the interfacial reactions leading to the formation of oxygen-and fluorine-containing byproducts. Notably, the Cu content in the pure Cu and low-Zn alloy samples decreased significantly, accompanied by a pronounced increase in O and F contents, indicating poor corrosion resistance. In contrast, the Cu-Zn (9:1 wt%) film better retained its elemental Cu proportion, suggesting that the incorporation of Zn helps to mitigate corrosion. Furthermore, the Cu-Zn (9:1 wt%)@C composite film retained a strong C signal post-corrosion and exhibited a lower degree of Cu depletion, demonstrating that the carbon coating effectively obstructs HF ingress and suppresses the formation of byproducts. The trends in elemental composition changes reveal that while the pre-corrosion samples were predominantly composed of their constituent base elements, the post-corrosion samples universally incorporated impurity elements such as O, F, and P, corroborating an HF-induced corrosion process. Concurrently, these results demonstrate that

both alloying and carbon-coating strategies can significantly enhance the corrosion resistance of the copper film, with the carbon coating exhibiting the most superior protective effect.

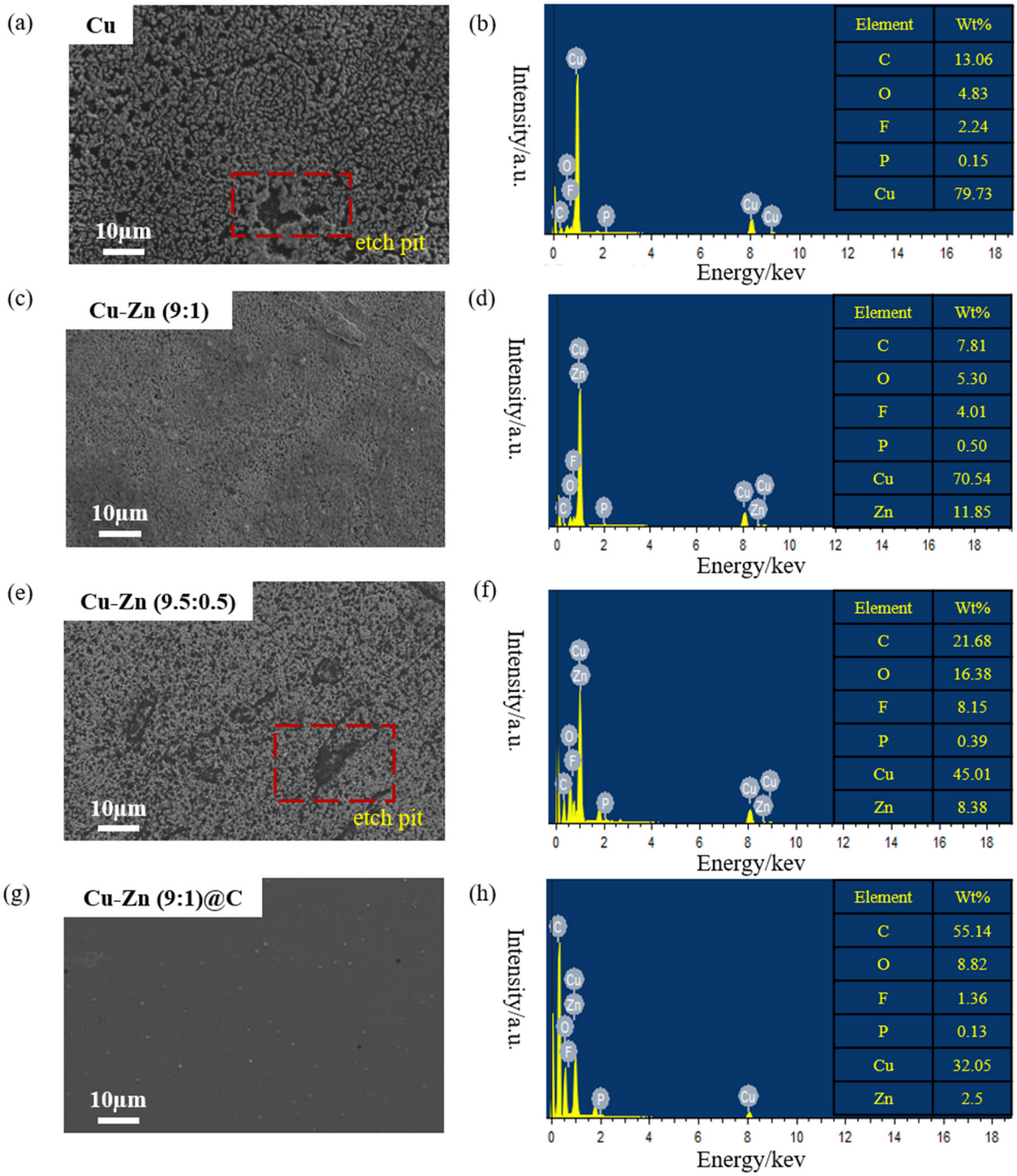

Figure 7. SEM images and EDS mapping of (**a**,**b**) Cu film, (**c**,**d**) Cu-Zn (9:1 wt%) film, (**e**,**f**) Cu-Zn (9.5:0.5 wt%) film, and (**g**,**h**) Cu-Zn (9:1 wt%)@C composite film after corrosion.

We further observed the evolution of the surface morphology of the samples before and after corrosion using a high-magnification optical microscope (1200×) (as shown in Figure 8). After the corrosion test, the pure Cu and Cu-Zn (9.5:0.5 wt%) films both exhibited distinct etch pits and morphological deterioration. In stark contrast, the surface of the Cu-Zn (9:1 wt%)@C composite film remained highly smooth and intact after undergoing the same corrosion process. Therefore, these results collectively confirm that the Cu-Zn (9:1 wt%)@C composite film possesses both good film-substrate adhesion and excellent corrosion resistance.

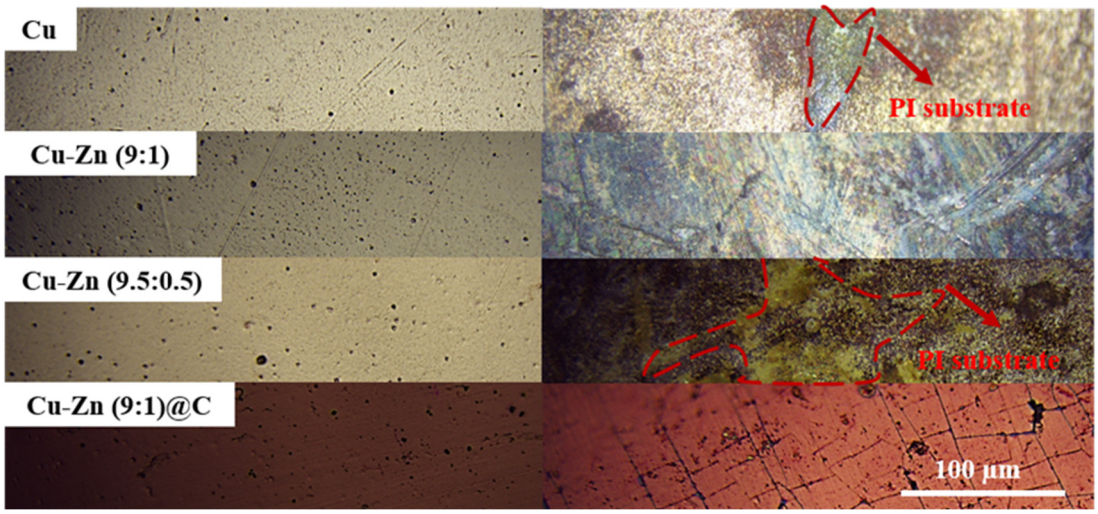

Figure 8. Comparison of surface morphologies of Cu film, Cu-Zn (9:1 wt%) film, Cu-Zn (9.5:0.5 wt%) film, and Cu-Zn (9:1 wt%)@C composite film before and after corrosion by optical microscopy.

To investigate the corrosion products and mechanisms, XRD was employed to analyze the crystal structure of all corroded samples, while XPS was further utilized to probe the surface chemical states of the optimized Cu-Zn (9:1 wt%)@C composite film. In the XRD diffraction pattern of the pure Cu film sample after prolonged corrosion, in addition to the characteristic diffraction peaks at (111), (200), and (220) corresponding to Cu, a characteristic peak appeared at 36° corresponding to the (111) crystal plane of a porous copper oxide species (PDF Card: 05-0667) (Figure 9a). This indicates that copper is easily oxidized in the electrolyte to form a fluffy, porous, and unstable copper oxide surface layer. For the Cu-Zn (9.5:0.5 wt%) film sample prepared with a small amount of Zn, the characteristic peaks of Cu almost disappeared after corrosion (Figure 9c), indicating its poor corrosion resistance and that its crystal structure was severely damaged during the corrosion process. This is attributed to the collapse of the overall structure caused by rapid de-zincification, which results from localized galvanic corrosion dnduced by micro-cell effects and microstructural non-uniformity.In contrast, the Cu-Zn (9:1 wt%) film sample with a higher Zn content largely maintained its peak profile, with only faint diffraction peaks of copper oxide species appearing. This is attributed to the increased Zn content reducing the galvanic effect and the slow leaching of Zn, which leads to the formation of a CuO or ZnO composite passivation film. This film, to a certain extent, prevents the oxidation of the substrate, resulting in corrosion resistance superior to that of pure Cu and Cu-Zn (9.5:0.5 wt%) film. Notably, for the Cu-Zn (9:1 wt%)@C composite film (Figure 9d), its XRD patterns before and after corrosion were almost identical, with only an extremely weak signal from copper oxide species detected. This shows that the inert carbon layer can minimize the interaction between the substrate and the electrolyte through various mechanisms, such as physical isolation and stress relief. This makes its corrosion resistance significantly superior to that of the Cu-Zn (9:1 wt%) film and far superior to those of the pure Cu film and the Cu-Zn (95:5 wt%) film.

Furthermore, XPS was conducted on the corroded surface of the optimized Cu-Zn (9:1 wt%)@C composite film to provide supplementary information regarding the surface chemical states of the carbon-protected film and the corrosion-related species formed after exposure to the electrolyte. As shown in its high-resolution Cu 2p spectrum in Figure 9f, a distinct Cu^{2+} characteristic doublet appears at 934.8 eV and 954.4 eV, while Cu or Cu^{+} components are present near 952.5 eV and 933 eV. This indicates the coexistence of metallic or subvalent copper and a small amount of divalent copper on the surface layer, which is attributed to the formation of Cu_2O and CuO products from corrosion. The high-resolution Zn 2p spectrum (Figure 9h) exhibits characteristic peaks assigned to Zn^{2+} at 1021.3 eV and 1045.7 eV, along with the presence of weak shoulder peaks for Zn^{0} (1044.3 eV and 1021.0 eV). This suggests that during the corrosion

process, Zn is partially leached out to form ZnO. The high-resolution F 1s spectrum displays characteristic peaks at 687.1 eV, 686.8 eV, and 686.1 eV, which are assigned, respectively, to the C-F (in CF_x), Cu^{2+}-F (in CuF_2), and Cu^{+}-F components. This is attributed to the hydrolysis of $LiPF_6$ in the electrolyte during the corrosion of Cu-Zn (9:1 wt%)@C composite film, which generates phosphate ions and the primary corrosive agent, HF. Therein, HF is first consumed by reacting with the outer carbon layer to form CF_x, and then it preferentially reacts with the more active Zn, thereby reducing the accessibility of HF to the main Cu current collector. EDS elemental mapping results further corroborate this, showing that on the corroded Cu-Zn (9:1 wt%)@C composite film, C and Cu elements are uniformly distributed, with small amounts of O, P, and F elements also present. These correspond to trace corrosion products such as CuO/ZnO, CuF_2, and phosphate species adhered to the surface. The above results indicate that the constructed hierarchical structure effectively mitigates the corrosion of the Cu current collector body. Consequently, the Cu-Zn (9:1 wt%)@C composite film exhibits the best corrosion resistance, which is consistent with the electrochemical results.

In order to further verify the effect of alloying itself on the chemical state of corrosion products and clarify the additional protection effect of the carbon layer, the XPS full spectrum analysis of the uncoated Cu-Zn (9:1 wt%) film after corrosion was carried out, and it was directly compared with the test results of the Cu-Zn (9:1 wt%)@C composite film, as shown in Figure 9i. The comparison results show that the introduction of the carbon layer significantly inhibits the corrosion of the corrosive medium. Specifically, the uncoated carbon Cu-Zn (9:1 wt%) film exhibits a strong F1s signal at ~686 eV, indicating that HF has a violent reaction with the alloy substrate, and a large number of CuF_2, ZnF_2 and other fluoride corrosion products are generated on the surface; in the Cu-Zn (9:1 wt%)@C composite film, the intensity of the F1s peak was significantly weakened, indicating that the dense carbon layer effectively blocked the penetration of HF into the alloy matrix and greatly inhibited the fluorination corrosion reaction. At the same time, the O1s signal of the uncoated sample is also significantly higher than that of the carbon-coated sample, indicating that more CuO/ZnO oxidation corrosion products are formed on the surface of the substrate without carbon layer protection. The physical isolation of the carbon layer effectively reduces the direct contact between the substrate and the oxygen/water-containing electrolyte. In addition, the C1s peak in the carbon-coated sample is extremely strong, while the matrix signals of Cu 2p and Zn 2p are relatively weak, which confirms that the carbon layer remains completely covered after corrosion and effectively protects the alloy matrix below. In contrast, the Cu 2p and Zn 2p signals from the uncoated carbon samples are directly exposed, indicating that there is no effective surface barrier. In summary, the above comparison results directly prove that although the Cu-Zn (9:1 wt%) alloy itself has a certain corrosion resistance foundation through solid solution strengthening and in-situ composite passivation layer, the external barrier effect of the carbon layer can further significantly inhibit HF erosion and oxidation corrosion, so that the Cu-Zn (9:1 wt%)@C composite film exhibits better chemical stability in a fluorine-containing electrolyte environment.

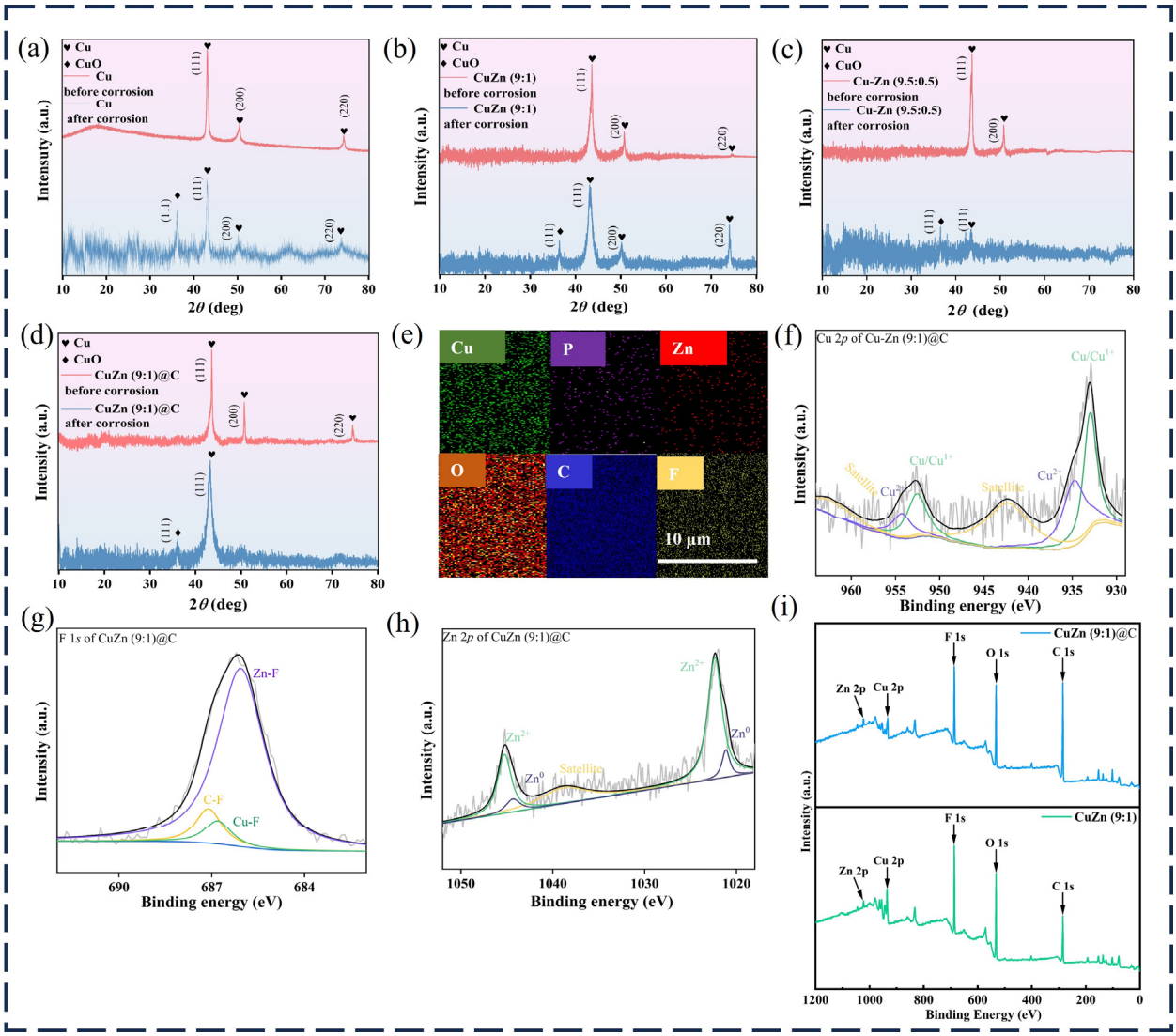

Figure 9. Structural and compositional analysis of the products on different composite films before and after corrosion: (**a**–**d**) Comparison of XRD patterns for the Cu film, Cu-Zn (9:1 wt%) film, Cu-Zn (9.5:0.5 wt%) film, and Cu-Zn (9:1 wt%)@C composite film s before and after corrosion; (**e**) EDS elemental distribution map of the surface layer of the Cu-Zn (9:1 wt%)@C composite film after corrosion; (**f**) High-resolution Cu 2p spectrum of the Cu-Zn (9:1 wt%)@C composite film after corrosion; (**g**) High-resolution F 1s spectrum of the Cu-Zn (9:1 wt%)@C composite film after corrosion; (**h**) High-resolution Zn 2p spectrum of the Cu-Zn (9:1 wt%)@C composite film after corrosion; (**i**) The full spectrum of Cu-Zn (9:1 wt%) is compared with that of Cu-Zn (9:1 wt %)@C.

3.5. Mechanistic Analysis of Corrosion

The variation in surface roughness before and after corrosion provides a quantitative basis for evaluating the corrosion resistance of the different films. As shown in Figure 10, the pure Cu film underwent significant roughening, with its average roughness (Ra) value increasing from 16.25 nm to 69.15 nm post-corrosion. The emergence of a CuO peak in its XRD pattern confirms that its surface was covered by corrosion byproducts. By contrast, the Cu-Zn (9:1 wt%) film exhibited a much smaller increase in its Ra value from 19.31 nm to 44.36 nm. This substantially smaller change in roughness demonstrates that alloying can effectively enhance the corrosion resistance of the composite films. This improvement is attributed to the solid solution strengthening effect imparted by an appropriate concentration of Zn, which facilitates the *in-situ* formation of a Cu-Zn composite oxide layer during the initial stages of corrosion. This layer is denser and more stable than the CuO formed on pure copper, thereby effectively retarding the corrosion process. Conversely, the Ra value of the Cu-Zn (9.5:0.5 wt%) film experienced a drastic increase from 8 nm to

151.19 nm. This phenomenon stems from an unfavorable compositional ratio, which leads to phase instability and microscopic phase separation. The formation of numerous micro-galvanic cells between the Cu-rich and the minority Zn-rich regions accelerates the anodic dissolution of zinc, inducing severe material degradation. Consequently, the order of corrosion resistance can be established as: Cu-Zn (9:1 wt%) > Cu > Cu-Zn (9.5:0.5 wt%).

Building on this, a carbon coating was introduced to further enhance corrosion resistance. The Ra value of the Cu-Zn (9:1 wt%)@C composite film remained virtually unchanged after corrosion, increasing only marginally from 1.71 nm to 1.91 nm, which indicates that its surface integrity was almost perfectly preserved. The primary mechanism for this enhancement lies in the multi-faceted protective role of the carbon layer. On one hand, SEM and EDS analyses confirm that the carbon layer is continuous, dense, and chemically inert, enabling it to effectively obstruct the infiltration of corrosive media such as HF. This is consistent with the XRD results, which detected no CuO peaks on the sample post-corrosion. On the other hand, the carbon layer does not participate in electrochemical reactions and therefore does not introduce new local galvanic potential differences, which guarantees the chemical stability of the interface. The synergistic effect of the stable solid solution formed by alloying, combined with the physical isolation provided by the carbon layer, allows the Cu-Zn (9:1 wt%)@C composite film to maintain a nearly pristine surface state even within a harsh corrosive environment. This demonstrates corrosion resistance superior to all of the uncoated samples.

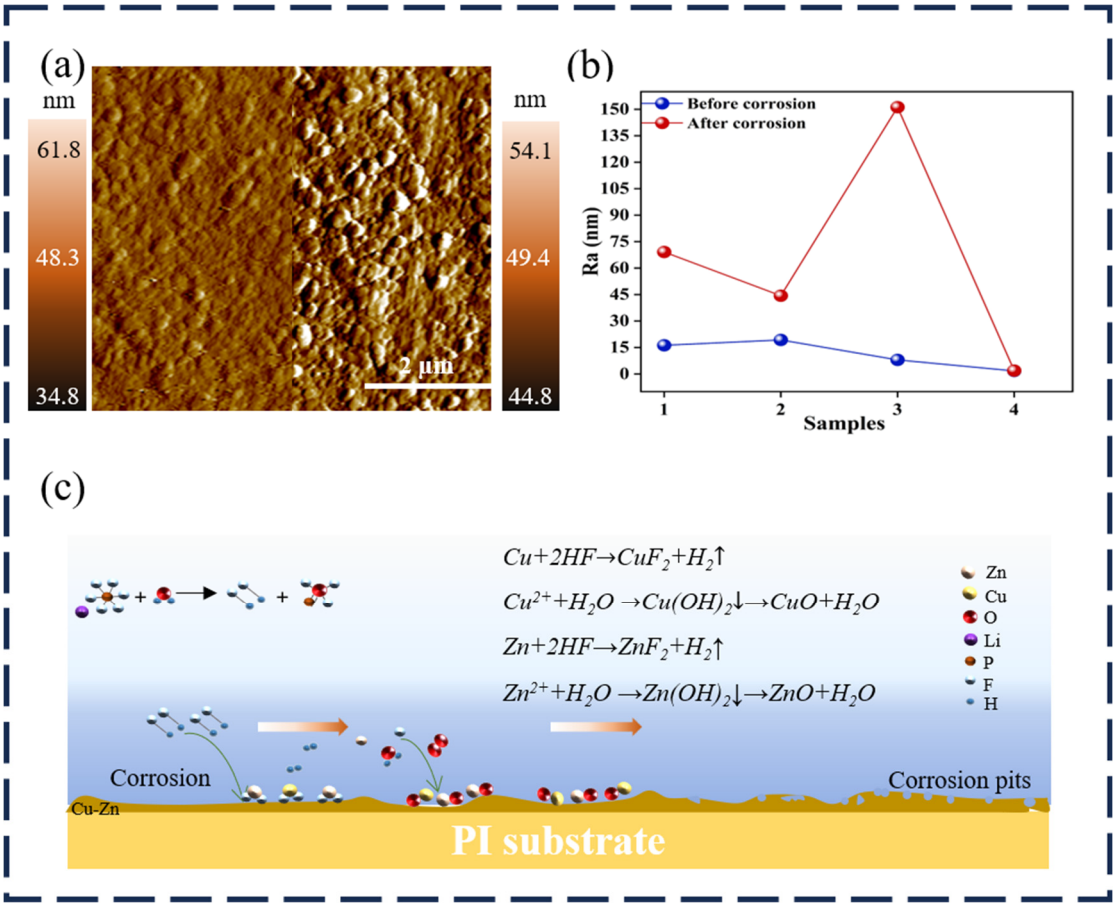

Figure 10. (**a**) Comparison of the 3D AFM surface morphologies for the Cu-Zn (9:1 wt%)@C composite film before and after corrosion; (**b**) Comparison of the surface roughness (Ra) for the different composite films before and after corrosion; (**c**) Schematic illustration of the corrosion reaction mechanism for a Cu-Zn film in an HF-containing electrolyte.

4. Conclusions

This study, focusing on the corrosion of copper alloy composite films in an HF-containing electrolyte, proposes a dual protective strategy of "alloying + carbon coating" and systematically elucidates its corrosion resistance mechanism by multi-scale characterization. Grounded in rigorous experimental design and quantitative analysis of multiple control groups, this work not only validates the better stability of the Cu-Zn (9:1 wt%)@C composite film but also establishes an empirical and theoretical foundation for designing metallic films for complex electrochemical environments. Synthesizing the theoretical framework, our experimental data, and established findings in the field, we can draw the following conclusions:

(1) SEM/EDS Characterization revealed significant differences in the surface morphology and composition of different films before and after corrosion. After corrosion, both the pure Cu and Cu-Zn (9.5:0.5 wt%) film exhibited evident etch pits and a sharp decrease in Cu content, accompanied by the enrichment of O and F elements. In contrast, the Cu-Zn (9:1 wt%) film showed only minor corrosion traces and retained a higher Cu content. The Cu-Zn (9:1 wt%)@C composite film, however, maintained a highly consistent elemental distribution and surface integrity before and after corrosion, demonstrating that the carbon layer can effectively block HF penetration.

(2) EIS and Tafel Results indicated a clear hierarchy in the corrosion resistance of the different films. The R_{ct} of pure Cu was only 6.76×10^3 $\Omega \cdot cm^2$, showing limited corrosion resistance. For the Cu-Zn (9.5:0.5 wt%) film, this was exacerbated by a micro-galvanic effect, causing its R_{ct} to decrease further to 1.24×10^3 $\Omega \cdot cm^2$, thereby exhibiting the poorest performance. Conversely, the Cu-Zn (9:1 wt%) composite film formed a dense composite passivation film, which increased its R_{ct} to 1.22×10^4 $\Omega \cdot cm^2$ and reduced its corrosion current density to 2.08×10^{-5} $mA \cdot cm^{-2}$. With the further introduction of a carbon coating, the corrosion current density of the Cu-Zn (9:1 wt%)@C composite film was further reduced to 6.14×10^{-6} $mA \cdot cm^{-2}$, with its roughness remaining almost unchanged, demonstrating the best stability.

(3) XRD/XPS Analysis showed that pure Cu was oxidized to form porous CuO species and CuF_2 by-products, leading to rapid interfacial degradation. The Cu-Zn (9.5:0.5 wt%) film suffered structural damage due to the localized and rapid dissolution of Zn. The Cu-Zn (9:1 wt%) film, however, formed a composite passivation layer during the gradual leaching of Zn, which helped to retard corrosion. For the Cu-Zn (9:1 wt%)@C composite film, under the protection of the carbon layer, HF preferentially reacted with carbon and Zn, leaving the Cu matrix barely involved in the corrosion reaction. This validates the dual synergistic mechanism of "internal passivation + external barrier".

(4) By systematically reviewing the existing literature and critically examining our results from multiple perspectives, we have distilled the following key findings: Alloying imparts inherent corrosion resistance to the substrate, while the carbon coating provides a functional external barrier. Their synergistic action significantly suppresses the HF-induced formation of by-products and interfacial degradation. Consequently, the Cu-Zn (9:1 wt%)@C composite film exhibits optimal corrosion resistance due to these multiple interacting mechanisms. This strategy offers an effective pathway for enhancing the long-term service stability of Cu-based materials in flexible electronics and energy storage systems.

Author Contributions

Conceptualization, D.J. and K.J.; Methodology, Y.F. (Yongqiang Fu); Software, Y.F. (Ying Fu); Validation, K.J.; Formal Analysis, K.J.; Investigation, K.J.; Resources, K.J.; Data Curation, K.J.; Writing—Original Draft Preparation, K.J.; Writing—Review & Editing, Y.Z.; Visualization, K.J.; Supervision, X.Z., X.C., T.L. and X.W.; Project Administration, D.J.; Funding Acquisition, D.J. and Y.F. (Yongqiang Fu).

Ethics Statement

Not applicable.

Informed Consent Statement

Not applicable.

Data Availability Statement

Data will be made available on request.

Funding

The APC was funded by author. This research was funded by the Key-Area Research and Development Program of Guangdong Province, grant number 2024B0101080003; the Jinzhou Key Research and Development Program, grant number JZ2024A019; the National Natural Science Foundation of China, grant number 52205204; and the Shandong Province Higher Education Institutions Youth Innovation Team Project, grant number 2023KJ116. The APC was funded by the authors.

Declaration of Competing Interest

The authors declare that they have no known competing financial interests or personal relationships that could have appeared to influence the work reported in this paper.

References

1. Katona RM, Karasz EK, Schaller RF. A Review of the Governing Factors in Pit-to-Crack Transitions of Metallic Structures. *Corrosion* **2023**, *79*, 72–96. DOI:10.5006/4179
2. Milošev I, Taheri P, Kapun B, Kozlica DK, Mol A, Kokalj A. The effect of molecular structure of imidazole-based compounds on corrosion inhibition of Cu, Zn, and Cu-Zn alloys. *Corros. Sci.* **2024**, *240*, 112328. DOI:10.1016/j.corsci.2024.112328
3. Akpanyung KV, Loto RT. Pitting corrosion evaluation: A review. *J. Phys. Conf. Ser.* **2019**, *1378*, 022088. DOI:10.1088/1742-6596/1378/2/022088
4. Shi F, Song Z, Ross PN, Somorjai GA, Ritchie RO, Komvopoulos K. Failure mechanisms of single-crystal silicon electrodes in lithium-ion batteries. *Nat. Commun.* **2016**, *7*, 11886. DOI:10.1038/ncomms11886
5. Andreeva VV. Behavior and Nature of Thin Oxide Films on Some Metals in Gaseous Media and in Electrolyte Solutions. *Corrosion* **1964**, *20*, 35t–46t. DOI:10.5006/0010-9312-20.2.35t
6. Peng Y, Feng X, Zhu Z, Xia J, Zhang W, Zhang F, et al. Study on the Commercial Metalized Plastic Current Collector PET-Cu and PP-Cu Toward High-Energy Lithium-Ion Battery. *Small* **2024**, *20*, 2405534. DOI:10.1002/smll.202405534
7. Qin R, Hu M, Zhang N, Guo Z, Yan Z, Li J, et al. Flexible Fabrication of Flexible Electronics: A General Laser Ablation Strategy for Robust Large-Area Copper-Based Electronics. *Adv. Electron. Mater.* **2019**, *5*, 1900365. DOI:10.1002/aelm.201900365
8. Chen J, Wang X, Gao H, Yan S, Chen S, Liu X, et al. Rolled electrodeposited copper foil with modified surface morphology as anode current collector for high performance lithium-ion batteries. *Surf. Coat. Technol.* **2021**, *410*, 126881. DOI:10.1016/j.surfcoat.2021.126881
9. Obrovac MN, Chevrier VL. Alloy Negative Electrodes for Li-Ion Batteries. *Chem. Rev.* **2014**, *114*, 11444–11502. DOI:10.1021/cr500207g
10. Pei A, Zheng G, Shi F, Li Y, Cui Y. Nanoscale Nucleation and Growth of Electrodeposited Lithium Metal. *Nano Lett.* **2017**, *17*, 1132–1139. DOI:10.1021/acs.nanolett.6b04755
11. Burzyńska L, Maraszewska A, Zembura Z. The corrosion of Cu-47.3 at% Zn BRASS in aerated 1.0 M HCl. *Corros. Sci.* **1996**, *38*, 337–347. DOI:10.1016/0010-938X(96)00132-1
12. Gaber GA, Soliman MM, Nasr ZA, Hyba AM. Comprehensive investigation of sustainable corrosion inhibitors on Cu–Zn alloy in simulated cooling water: Electrochemical explorations, SEM/EDX analysis, and DFT/molecular simulations

utilizing expired Bepotastine-B as a green inhibitor. *Sustain. Chem. Pharm.* **2024**, *37*, 101340. DOI:10.1016/j.scp.2023.101340
13. Shahzad RF, Rasul S, Mamlouk M, Lukose CC, Shakoor RA, Zia AW. Innovative Tin and hard carbon architecture for enhanced stability in lithium-ion battery anodes. *J. Energy Storage* **2024**, *100*, 113671. DOI:10.1016/j.est.2024.113671
14. Peng Z, Ding D, Zhang W, Gao Y, Chen G, Xie Y, et al. Tensile Property and Corrosion Performance of Ag Microalloying of Al-Cu Alloys for Positive Electrode Current Collectors of Li-Ion Batteries. *Materials* **2022**, *15*, 5126. DOI:10.3390/ma15155126
15. Wang P, Zhang K, Hu J, Zheng M. A Cu-Zn bimetallic organic framework as protective interlayer for dendrite-free Zn deposition in zinc-based flow batteries. *Electrochim. Acta* **2024**, *504*, 144949. DOI:10.1016/j.electacta.2024.144949
16. Kanimozhi SN, Vasudevan B, Souwaileh AA, Subbiah J, Anandan S. Cu-Zn layered double hydroxides as high-performance electrode for supercapacitor applications. *Electrochim. Acta* **2024**, *507*, 145106. DOI:10.1016/j.electacta.2024.145106
17. Taylor AH. The Corrosion Behavior of Cu and Naval Brass in 0.5M NaCl Solutions at Ambient Temperature. *J. Electrochem. Soc.* **1971**, *118*, 854. DOI:10.1149/1.2408204
18. Pickering HW, Byrne PJ. Partial Currents During Anodic Dissolution of Cu-Zn Alloys at Constant Potential. *J. Electrochem. Soc.* **1969**, *116*, 1492. DOI:10.1149/1.2411582
19. Fenelon AM, Breslin CB. An Electrochemical study of the formation of Benzotriazole surface films on Copper, Zinc and a Copper–Zinc alloy. *J. Appl. Electrochem.* **2001**, *31*, 509–516. DOI:10.1023/A:1017503031045
20. Milošev I, Mikić TK, Gaberšček M. The effect of Cu-rich sub-layer on the increased corrosion resistance of Cu–xZn alloys in chloride containing borate buffer. *Electrochim. Acta* **2006**, *52*, 415–426. DOI:10.1016/j.electacta.2006.05.024
21. Mikić TK, Milošev I, Pihlar B. Passivity and Corrosion of Cu–xZn (x = 10–40 wt%) Alloys in Borate Buffer Containing Chloride Ions. *J. Appl. Electrochem.* **2005**, *35*, 975–984. DOI:10.1007/s10800-005-6726-x
22. Song QN, Xu N, Bao YF, Jiang YF, Gu W, Yang Z, et al. Corrosion Behavior of Cu40Zn in Sulfide-Polluted 3.5% NaCl Solution. *J. Mater. Eng. Perform.* **2017**, *26*, 4822–4830. DOI:10.1007/s11665-017-2940-z
23. Milošev I. The effect of various halide ions on the passivity of Cu, Zn and Cu–xZn alloys in borate buffer. *Corros. Sci.* **2007**, *49*, 637–653. DOI:10.1016/j.corsci.2006.06.009
24. Ali SM, Roohan Farooq Lala S, Golla BR. Corrosion behavior of mechanically alloyed Cu-Zn and Cu-15Al-Zn alloys in NaCl environment. *J. Alloys Compd.* **2025**, *1041*, 183876. DOI:10.1016/j.jallcom.2025.183876
25. Kim HR, Choi WM. Graphene modified copper current collector for enhanced electrochemical performance of Li-ion battery. *Scr. Mater.* **2018**, *146*, 100–104. DOI:10.1016/j.scriptamat.2017.11.030
26. Khamseh S, Alibakhshi E, Mahdavian M, Saeb MR, Vahabi H, Kokanyan N, et al. Magnetron-sputtered copper/diamond-like carbon composite thin films with super anti-corrosion properties. *Surf. Coat. Technol.* **2018**, *333*, 148–157. DOI:10.1016/j.surfcoat.2017.11.012
27. Han CM. Advances in Carbon Coatings for Current Collectors in Lithium-Ion Battery Applications: Focus on Three-Dimensional Carbon Nanowalls. *Coatings* **2025**, *15*, 86. DOI:10.3390/coatings15010086
28. Fu Y, Zhou F, Wang Q, Zhang M, Zhou Z. Electrochemical and tribocorrosion performances of CrMoSiCN coating on Ti-6Al-4V titanium alloy in artificial seawater. *Corros. Sci.* **2020**, *165*, 108385. DOI:10.1016/j.corsci.2019.108385
29. Fu Y, Zhou F, Zhang M, Wang Q, Zhou Z. Structural, mechanical and tribocorrosion performances of CrMoSiN coatings with various Mo contents in artificial seawater. *Appl. Surf. Sci.* **2020**, *525*, 146629. DOI:10.1016/j.apsusc.2020.146629
30. Fu Y, Zhou F, Feng J, Luo H, Zhang M. Long-term corrosion resistance and friction-induced antibacterial enhancement of CrMoSiCN coating on Ti6Al4V alloy. *Corros. Sci.* **2021**, *186*, 109478. DOI:10.1016/j.corsci.2021.109478
31. Choudhury R, Wild J, Yang Y. Engineering current collectors for batteries with high specific energy. *Joule* **2021**, *5*, 1301–1305. DOI:10.1016/j.joule.2021.03.027
32. Ye Y, Chou LY, Liu Y, Wang H, Lee HK, Huang W, et al. Ultralight and fire-extinguishing current collectors for high-energy and high-safety lithium-ion batteries. *Nat. Energy* **2020**, *5*, 786–793. DOI:10.1038/s41560-020-00702-8
33. Zhang Z, Song Y, Zhang B, Wang L, He X. Metallized Plastic Foils: A Promising Solution for High-Energy Lithium-Ion Battery Current Collectors. *Adv. Energy Mater.* **2023**, *13*, 2302134. DOI:10.1002/aenm.202302134
34. Bao W, Wang R, Sun K, Qian C, Zhang Y, Li J. Interface Crystallographic Optimization of Crystal Plane for Stable Metallic Lithium Anode. *ACS Appl. Mater. Interfaces* **2022**, *14*, 38696–38705. DOI:10.1021/acsami.2c08278
35. Li H, Wang L, Song Y, Zhang Z, Zhang H, Du A, et al. Significance of Current Collectors for High Performance Conventional Lithium-Ion Batteries: A Review. *Adv. Funct. Mater.* **2023**, *33*, 2305515. DOI:10.1002/adfm.202305515
36. Toki GFI, Hossain MK, Rehman WU, Manj RZA, Wang L, Yang J. Recent progress and challenges in silicon-based anode materials for lithium-ion batteries. *Ind. Chem. Mater.* **2024**, *2*, 226–269. DOI:10.1039/D3IM00115F

37. Huo S, Wang L, Su B, Xue W, Wang Y, Zhang H, et al. Anode-Free Li Metal Batteries: Feasibility Analysis and Practical Strategy. *Adv. Mater.* **2024**, *36*, 2411757. DOI:10.1002/adma.202411757
38. Zheng S, Ding L, Hu F, Zhang Y, Ouyang Z, Yang S. Construction of PES composite ultrafiltration membrane with high permeability and selectivity assisted by three-dimensional Ni-Zn MOF@Multi CNC. *Sep. Purif. Technol.* **2025**, *354*, 129091. DOI:10.1016/j.seppur.2024.129091
39. Sun H, He X, Ren J, Li J, Jiang C, Wan C. Hard carbon/lithium composite anode materials for Li-ion batteries. *Electrochim. Acta* **2007**, *52*, 4312–4316. DOI:10.1016/j.electacta.2006.12.012
40. Liu J, Jia H, Nguyen D, Liu J, Fang C. Fabricating ultralight and ultrathin copper current collectors for high-energy batteries. *eScience* **2024**, *4*, 100271. DOI:10.1016/j.esci.2024.100271
41. Almonti D, Salvi D, Ucciardello N, Vesco S. Enhanced Wear Resistance and Thermal Dissipation of Copper–Graphene Composite Coatings via Pulsed Electrodeposition for Circuit Breaker Applications. *Materials* **2024**, *17*, 6017. DOI:10.3390/ma17236017
42. Wang J, Guo LN, Lin WM, Chen J, Zhang S, Chen SD, et al. The effects of graphene content on the corrosion resistance, and electrical, thermal and mechanical properties of graphene/copper composites. *New Carbon Mater.* **2019**, *34*, 161–169. DOI:10.1016/S1872-5805(19)60009-0